

CORE: Compensable Reward as a Catalyst for Improving Offline RL in Wireless Networks

Lipeng Zu¹, Hansong Zhou¹, Yu Qian¹, Shayok Chakraborty¹, Yukun Yuan², Linke Guo³, Xiaonan Zhang¹

¹Florida State University, USA

²University of Tennessee at Chattanooga, USA

³Clemson University, USA

Abstract—Real-world wireless data are expensive to collect and often lack sufficient expert demonstrations, causing existing offline RL methods to overfit suboptimal behaviors and exhibit unstable performance. To address this issue, we propose CORE, an offline RL framework specifically designed for wireless environments. CORE identifies latent expert trajectories from noisy datasets via behavior embedding clustering, and trains a conditional variational autoencoder with a contrastive objective to separate expert and non-expert behaviors in latent space. Based on the learned representations, CORE constructs compensable rewards that reflect expert-likeness, effectively guiding policy learning under limited or imperfect supervision. More broadly, this work represents one of the early systematic explorations of offline RL in wireless networking, where prior adoption remains limited. Beyond introducing offline RL techniques to this domain, we further examine intrinsic wireless data characteristics and develop a domain-aligned algorithm that explicitly accounts for their structural properties. While offline RL has not yet been fully established as a standard methodology in the wireless community, our study aims to provide foundational insights and empirical evidence to support its broader acceptance.

Index Terms—Offline Reinforcement Learning, Network Management, Resource Allocation, Edge Computing

I. INTRODUCTION

A. Background: RL in Wireless Networks

Next-generation wireless networks are expected to support significantly higher data rates, lower latency, and a massive number of connected devices. Meeting these requirements poses significant challenges for network control, as wireless environments are becoming increasingly dynamic and difficult to model. Traditional rule-based and optimization-driven approaches fall short under such conditions, due to their reliance on static models and fixed heuristics [1]. In contrast, learning-based methods offer greater flexibility by adapting to changing environments and extracting actionable patterns from data. Among them, reinforcement learning (RL) has shown strong potential for sequential decision-making, with demonstrated success in tasks such as spectrum allocation [2], network scheduling [3], and edge offloading [4].

Despite its promise, existing RL approaches in wireless networks rely on online interaction with the environment, where the agent continuously updates its policy through trial-and-error learning [5]. Online exploration in dynamic and safety-critical wireless environments can cause unstable behavior, degraded quality of service, or even service disruptions [6]. Offline RL offers a promising alternative by enabling policy

learning from pre-collected datasets without requiring further environmental interactions. By avoiding unsafe exploration, offline RL significantly reduces deployment risks and is particularly well-suited for real-world wireless tasks [7].

However, the reliance on pre-collected datasets renders offline RL vulnerable to distributional shifts and coverage bias. For instance, a spectrum allocation policy trained on low-interference campus data often fails under heavy urban interference. Similarly, an offloading agent that has never encountered peak-hour traffic loads struggles to handle high server utilization. These mismatches result in out-of-distribution (OOD) issues during policy deployment. Under these conditions, the learned policy encounters unfamiliar regions of the state-action space and is forced to extrapolate, which can lead to erratic or suboptimal behavior [8]. In safety-critical wireless systems such as industrial automation or real-time medical monitoring, incorrect decisions caused by OOD inputs can cause equipment failure, mission-critical service breakdowns, or even threats to human safety. Therefore, we raise a critical question: *how can we effectively learn reliable policies from limited and potentially biased offline data?* Addressing this question requires not only making efficient use of scarce samples but also enhancing generalization to unseen or underrepresented state-action pairs.

B. State of the Art and Challenges

Mitigating OOD risks in offline RL relies on identifying and leveraging high-quality *expert data* from the training dataset [9]. However, acquiring sufficient expert demonstrations is inherently difficult due to stringent privacy regulations and restricted access to operational network telemetry [10], [11]. As a more practical alternative, recent work explores *reward relabeling*, which reconstructs the reward structure across the dataset by propagating guidance from a small number of expert-labeled states and actions [12]. To enable robust offline policy learning in wireless networks, we identify and address two key challenges that hinder the effectiveness of expert-based reward relabeling.

Challenge 1: Significant bias in trajectory-based expert identification. Reward relabeling typically begins by identifying expert trajectories within the dataset. A straightforward approach is to select samples with the highest trajectory returns as the expert. However, such a strategy often overrepresents idealized scenarios, failing to capture the diversity of real-

world wireless conditions. For the example of task offloading in multi-access computing networks, the trajectories with highest accumulated Quality of Service often correspond to periods with low server load and stable network connections. Treating them as expert data will fail to adapt to the frequent variations in server load and wireless conditions encountered during real-world operation.

Challenge 2 : Unclear distinction of expert and non-expert data in latent space. Recent methods employing Conditional Variational Autoencoders aim to learn latent representations that separate expert and non-expert trajectories [13]. These embeddings are then used to relabel rewards based on the proximity of an agent’s behavior to expert samples. However, non-expert data often overlaps significantly with expert data in the latent space, blurring the intended boundary. As a result, reward relabeling becomes less discriminative, offering only limited performance gains over baseline methods without expert guidance. Learning well-separated and structure-aware latent representations remains a fundamental challenge for building reliable expert-driven reward functions.

C. Present Work

Motivated by the observation that increased reward discrepancies within similar state groups lead to better training performance (Sec. III), we propose a novel framework named CORE (enhanced Conditional VAE for cOmpensable REwards) to directly address the above challenges by enhancing policy learning via enlarging reward discrepancies. Specifically, CORE answers two critical questions: (i) how to identify the expert samples (**Challenge 1**); and (ii) how to efficiently explore those identified expert samples (**Challenge 2**). To tackle the first question, CORE employs clustering to select samples with optimal rewards as the expert data. For the second question, CORE designs an enhanced Conditional Variational Autoencoder (CVAE) featuring a contrastive component integrated into its loss function. This contrastive enhancement enhances distinct clustering of expert samples in the latent space, which distinctly separates expert from non-expert samples. Furthermore, CORE applies compensable rewards across all samples to amplify distinctions between expert and non-expert behaviors. Given the lightweight design, CORE serves as a versatile and broadly applicable enhancement for various offline RL-based wireless network tasks.

We validate CORE with three mainstream wireless network use cases in real world. In the first one, we investigate the resource allocation in ORAN-Cloud with multiple available servers deployed within the centralized unit. The agent distributes incoming tasks to appropriate servers based on user demand, hardware status and task queue to maximize the system-wide QoS. The second one is to offload real-time object detection tasks from edge devices (NVIDIA Orin Nano) to the server (NVIDIA RTX 3060 Ti) for inference acceleration. The agent needs to balance latency and energy consumption by adjusting the offloading portions based on the system conditions. In the last one, we set up 2 USRP N210s to implement CSI-based adaptive random channel access for

data transmission using Wi-Fi protocol in dynamic network conditions. The superior performance exhibited by the CORE in the above use cases validates its effectiveness and robustness across a variety of practical wireless network tasks.

We summarize our key contributions as follows.

- We are the first work observing that increased reward discrepancies within intra-states lead to better training performance. Motivated by it, we propose CORE, an offline RL designed to improve learning efficiency.
- We propose a state-based expert identification method. Via selecting high-reward samples from clustered offline data, our method offers more effective expert guidance than existing trajectory-level approaches.
- We design a compensable reward mechanism. Through adjusting rewards based on the distance to expert behaviors in the latent space, our mechanism effectively amplifies the learning signals from limited offline dataset.
- We evaluate CORE using real-world data collected from various real wireless systems. Experiment results show that CORE significantly improves policy reliability and robustness across all practical wireless tasks.

II. PRELIMINARIES

A. Offline Reinforcement Learning

Reinforcement Learning (RL) involves an agent learning to optimize decisions within an environment [14], modeled as a Markov Decision Process (MDP), in which comprises a state space \mathcal{S} , an action space \mathcal{A} , a transition function ρ that denotes the probability of transitioning from state s to s' through action a , a reward function r that provides rewards interacting with environment, and a discount factor γ that evaluates the significance of future rewards.

Offline RL refers to the paradigm where the learning process is restricted to a pre-collected dataset of experiences [15]. Unlike the traditional online RL, where an agent iteratively collects data through interaction with the environment, offline RL assumes no further data collection is required. This assumption is crucial in domains where active exploration and data collection can be prohibitively expensive or risky, such as experimenting new spectrum-allocation policies in live cellular networks or allocation strategies in city-wide MEC networks.

B. Conditional VAE

Conditional Variational Autoencoder (CVAE) is a generative model that extends the Variational Autoencoder (VAE) by incorporating conditional variables. Mathematically, CVAE aims to maximize the Evidence Lower Bound (ELBO) on the conditional log-likelihood of observing an action given a state [16], formulated as follows:

$$\begin{aligned}
 \mathcal{L}_{\text{ELBO}}(s, a; \theta, \phi) &= \mathcal{L}_{\text{recon}} + \mathcal{L}_{\text{KL}} \\
 &= -\mathbb{E}_{q_{\phi}(\mathbf{z}|s, a)} [\log p_{\theta}(a|\mathbf{z}, s)] + \text{KL}(q_{\phi}(\mathbf{z}|s, a) \| p_{\theta}(\mathbf{z}|s)) \\
 &= -\frac{1}{L} \sum_{l=1}^L \log p_{\theta}(a|\mathbf{z}^{(l)}, s) + \text{KL}(q_{\phi}(\mathbf{z}|s, a) \| p_{\theta}(\mathbf{z}|s)),
 \end{aligned} \tag{1}$$

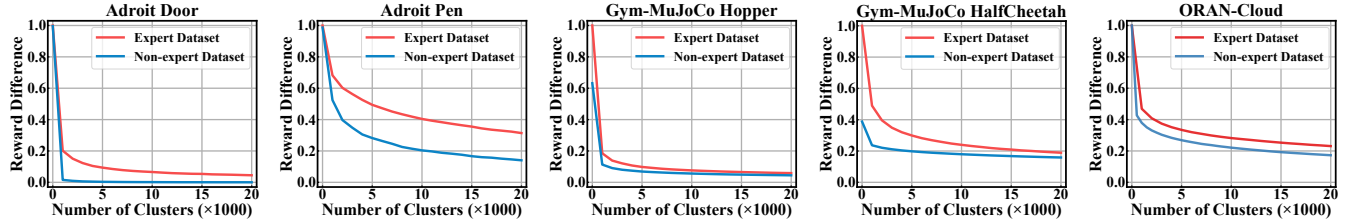


Fig. 1: Comparative analysis of offline datasets across various applications, generated by the expert policy and others. From left to right: Adroit (Door and Pen), Gym-MuJoCo (Hopper and HalfCheetah), and ORAN-Cloud.

where: $\mathcal{L}_{\text{recon}}$ and KL indicate the reconstruction loss and KL -divergence, respectively; \mathbf{z} is the latent variable encoded by the variational posterior $q_{\phi}(\mathbf{z}|\mathbf{s}, \mathbf{v}_a)$, parameterized by ϕ ; $p_{\theta}(a|\mathbf{z}, \mathbf{s})$ is the likelihood of reconstructing the action vectors given the latent variables and the state, parameterized by θ ; and $p_{\theta}(\mathbf{z}|\mathbf{s})$ represents the prior over the latent variables conditioned on the state. In practice, the latent variable \mathbf{z} in Eq. (1) can be resampled by:

$$\mathbf{z} = \mu + \sigma \cdot \epsilon, \quad (2)$$

where $\epsilon \sim \mathcal{N}(0, 1)$ infuses the model with random Gaussian noise. It is modulated by the latent distribution's standard deviation, σ .

III. MOTIVATION

Expert demonstrations are known to significantly improve the effectiveness of offline RL algorithms [17]. However, in wireless network tasks, it is often unclear whether available data truly reflects expert behavior. Unlike synthetic benchmarks, real-world wireless datasets are collected under fluctuating conditions and lack explicit performance labels, making expert identification inherently ambiguous. To better understand the distinguishing features between expert samples and non-expert samples, we conduct a comparative analysis across multiple offline tasks, including the standard offline RL benchmarks Adroit [18] and Gym-MuJoCo [19], and a wireless scenario, ORAN-Cloud. For the first two tasks, both expert and non-expert datasets¹ are obtained from the open-source benchmark D4RL [20]. Their non-expert datasets are collected via behavior cloning (Door and Pen) and random (Hopper and HalfCheetah). For ORAN-Cloud, the expert dataset are generated via a trained Proximal Policy Optimization (PPO) policy [21], while the non-expert data is obtained using a simple Round-Robin heuristic.

For each dataset, we cluster the state and measure the reward difference between the highest and lowest samples within each cluster. This metric captures the variability of rewards among behaviorally similar samples and serves as a proxy for local reward expressiveness. As shown in Fig. 1, expert datasets (red lines) consistently exhibit greater intra-cluster reward differences, indicating that expert data provides more detailed and informative reward signals for similar states. In contrast, reward differences in non-expert datasets (blue lines) diminish rapidly as the number of clusters increases, reflecting

a lack of useful learning signals. Since the reward discrepancy is positively correlated with the offline RL performance [22], such local reward diversity plays a critical role in policy effectiveness. These findings motivate the following insight:

Offline datasets with greater reward variation among similar states are more effective in guiding learning algorithms toward optimal behavior.

IV. METHOD

A. Framework Overview

We propose an enhanced Conditional Variational Autoencoder framework for Compensable Rewards (CORE), as illustrated in Fig. 2. The CORE framework begins by identifying expert samples from the offline dataset through clustering (Sec. IV-B). These expert and non-expert samples are then used to train a Conditional Variational Autoencoder (CVAE). To better separate expert and non-expert behaviors in the latent space, we integrate a contrastive loss into the CVAE objective, which enhances representation disentanglement and improves latent discriminability (Sec. IV-C). Once the model is trained, it estimates the latent distance between each data sample and the expert cluster centroid. This distance is treated as a compensable reward, which quantifies the behavioral proximity to expert demonstrations. By incorporating this reward into the original signal, CORE enables more effective offline policy learning (Sec. IV-D).

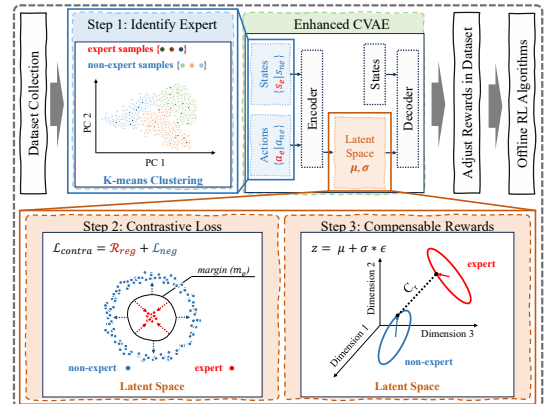


Fig. 2: Overview of our proposed framework CORE.

To address the challenge ① (Sec. IV-B), CORE deploys a large amount of clustering to partition the complex state space of the wireless environment in fine-coarse and select the corresponding expert data. This enables the RL agent to obtain more accurate high-quality anchor points when encountering

¹available at: http://rail.eecs.berkeley.edu/datasets/offline_rl/

new states during training. As for the challenge ② (Sec. IV-C), the designed contrastive loss and the compensable reward scheme significantly enhance the distinction between expert and non-expert data in the latent space. As depicted in Step 2 and Step 3 of Fig. 2, CORE reshapes the distribution patterns of these two types of data, thereby preventing ineffective utilization of expert samples during reward relabeling.

B. Expert Data Sampling

Our motivation in Sec. III shows that offline RL benefits from larger intra-cluster reward variation, where samples with similar states exhibit varying quality of behaviors. Hence, we first put the samples with similar states together, for which K-means is deployed for clustering over the state space \mathcal{S} . Within each cluster, we then select the top-performing samples with the highest rewards as expert samples, which form the expert datasets \mathcal{D}^e . The remaining samples are assigned to the non-expert dataset \mathcal{D}^{ne} . This ensures that the expert dataset captures diverse yet consistently high-performing behaviors across different regions of the state space. The resulting \mathcal{D}^e is thus enriched with near-optimal actions.

Justification. While trajectory-based clustering aligns more closely with the temporal structure of RL, it becomes unreliable in real-world offline datasets, which often contain limited or biased trajectories. In contrast, clustering based on individual states provides a practical alternative for identifying high-quality behaviors, especially when the data is sparse or covers ideal conditions. This makes state-based clustering more effective for guiding offline policy learning in dynamic wireless environments.

C. CVAE Enhancement with Contrastive Loss

1) *CVAE with Discrete Action Space*: In practical wireless network tasks like resource allocation and task scheduling, action spaces are discrete. To effectively learn from environments with discrete action spaces, we incorporate an embedding function, denoted as $Emb : \mathcal{A} \rightarrow \mathbb{R}^{d_{emb}}$. The model's output layer computes a vector $p_{\hat{a}} \in \mathbb{R}^{|\mathcal{A}|}$ via a fully connected layer over the entire action space \mathcal{A} . We then redefine $\mathcal{L}_{\text{recon}}$ in Eq. (1) as $\tilde{\mathcal{L}}_{\text{recon}}$ via a cross-entropy function between the likelihood of reconstructing $p_{\hat{a}}$ and the actual training actions. Specifically, given the predicted action distribution $p_{\theta}(p_{\hat{a}}|\mathbf{z}, s)$ for each state s and the actual action a taken from the training data, $\tilde{\mathcal{L}}_{\text{recon}}$ is given by:

$$\tilde{\mathcal{L}}_{\text{recon}} = -\frac{1}{L} \sum_{i=1}^L \sum_{j=1}^{|\mathcal{A}|} y_{ij} \log(p_{ij}), \quad (3)$$

where L is the batched sample size in the training loop and $p_{ij} = \text{softmax}(p_{\hat{a}})$. y_{ij} is a binary indicator that equals 1 if the action j is taken for the i -th sample, and 0 otherwise.

2) *Contrastive Loss Enhancement*: To segregate expert actions from non-expert ones and further structure the latent space by mixing dataset $\mathcal{D} = \mathcal{D}^e \cup \mathcal{D}^{ne}$, we incorporate a novel contrastive loss that consists of regularization loss and negative pair loss.

Regularization Loss, \mathcal{R}_{reg} , aims to improve model generalization by clustering expert action embeddings within the latent space, thus reducing their variance. It is defined as:

$$\mathcal{R}_{\text{reg}} = -\lambda_{\text{reg}} \cdot \text{std}(\dots, \mathbf{z}_e^j, \dots), \quad (4)$$

where the regularization coefficient λ_{reg} weights the importance of the regularization loss; and $\text{std}(\cdot)$ calculates the variance of the latent variables associated with expert state-action pairs $(s, a)_e$. The goal is to encourage a denser clustering of expert samples in the latent space, facilitating a more structured and organized representation of expert behaviors.

Negative Pair Loss, \mathcal{L}_{neg} , encourages a clear separation between the latent representations of expert (\mathbf{z}_e) and non-expert (\mathbf{z}_{ne}) samples, enabling the model to effectively distinguish between expert and non-expert knowledge. It is defined as:

$$\mathcal{L}_{\text{neg}} = -\lambda_{\text{neg}} \cdot \mathbb{E}_{e \sim \mathcal{D}^e, ne \sim \mathcal{D}^{ne}} [\max(0, m_e - \|\mathbf{z}_e - \mathbf{z}_{ne}\|_2)], \quad (5)$$

where the negative coefficient λ_{neg} weights the importance of the negative pair loss, and m_e is a predefined margin representing the minimum desired separation between expert and non-expert samples. \mathcal{L}_{neg} incentivizes the model to create a latent space where expert knowledge is not only distinct, but also spatially segregated from less expert knowledge.

3) *Overall Objective Function*: The overall objective function for the enhanced CVAE model, $\tilde{\mathcal{L}}_{\text{CVAE}}$, combines the CVAE loss $\mathcal{L}_{\text{CVAE}}$ with a contrastive loss $\mathcal{L}_{\text{contra}}$. The original loss function in Eq. (1) is redefined as:

$$\tilde{\mathcal{L}}_{\text{CVAE}} = \mathcal{L}_{\text{CVAE}} + \mathcal{L}_{\text{contra}} = \underbrace{\tilde{\mathcal{L}}_{\text{recon}} + \mathcal{L}_{\text{KL}}}_{\text{CVAE}} + \underbrace{\mathcal{R}_{\text{reg}} + \mathcal{L}_{\text{neg}}}_{\text{Contra. Loss}} \quad (6)$$

The integration of $\tilde{\mathcal{L}}_{\text{recon}}$ in Eq. (3), \mathcal{R}_{reg} in Eq. (7), and \mathcal{R}_{reg} in Eq. (5) into a unified objective function allows our model to not only generate high-fidelity data but also to discern and distinguish between nuanced differences in the data, enabling effective learning from complex, structured data spaces.

D. Compensable Reward

Inspired by intrinsic reward mechanisms [23], we design a compensable reward to guide the learning agent toward expert-aligned decisions while preserving alignment with the true task objective. Conventional intrinsic rewards, which serve as internal signals and entirely replace the environment reward [24], cannot be directly deployed in our framework. This is because the expert samples are likely to suffer from bias due to limited coverage or suboptimal demonstrations. Relying solely on these samples for reward relabeling can mislead the agent toward unintended or even undesirable behaviors.

To mitigate the bias introduced by expert samples, we retain the original reward signal as a stabilizing anchor to prevent overfitting. The contrastive loss has already encouraged expert samples to form a discriminative cluster in the latent space, pulling similar expert behaviors closer. The centroid of this cluster represents their overall decision pattern. For each sample in the dataset, we compute its latent representation and derive a compensable reward by measuring its distance to

the expert centroid. This compensable reward is then added to the original reward to guide policy learning.

Mathematically, the centroid of expert samples is calculated as the mean of the latent representations, which is:

$$\mathbf{z}_e^c = \frac{1}{N} \sum_{i=1}^N \mathbf{z}_e^i, \quad (7)$$

\mathbf{z}_e^i is the latent representation of the i -th expert sample $\in \mathcal{D}^e$; and N is the total number of \mathcal{D}^e . Eq. (7) captures a generalized representation of expert behavior within the latent space.

We further quantify the deviation of any sample's actions in \mathcal{D} from this expert centroid to determine how closely the agent's decisions align with those of the experts. This deviation, $\text{dist}(\mathbf{z}_x, \mathbf{z}_e^c)$, is defined by the Euclidean distance between the agent's action representation, \mathbf{z}_x , and the expert centroid, \mathbf{z}_e^c :

$$\text{dist}(\mathbf{z}_x, \mathbf{z}_e^c) = \|\mathbf{z}_x - \mathbf{z}_e^c\|_2. \quad (8)$$

A smaller distance indicates a desired higher degree of alignment with expert behaviors.

To compensate for deviations from the expert behavior, a compensation reward, C_r , is introduced to the original reward r_o . We modify the overall reward r_{adj} as:

$$r_{adj} = r_o + C_r = r_o - \tau \cdot \text{dist}(\mathbf{z}_x, \mathbf{z}_e^c), \quad (9)$$

where τ is a scaling factor that modulates the impact of deviation on the compensation reward.

Finally, we update the reward in the dataset, which are used for offline training. The update ensures that the learning agent is not only motivated by immediate task-specific objectives but also by the imperative to conform to expert-derived behaviors.

Analysis From Eq. (2), injecting Gaussian noise into the CVAE latent space transforms introduces deviations around the dataset-derived expert centroid, enabling the discovery of higher-reward actions closer to optimal policies. The inclusion of ϵ thus enhances exploration and aligns with directed search strategies in policy optimization [25], effectively recalibrating compensatory reward estimation.

V. APPLICATION TO PRACTICAL WIRELESS NETWORKS

To demonstrate the effectiveness of the CORE framework, we consider three representative wireless use cases for comprehensive empirical evaluation, including scalable and efficient resource allocation in ORAN-Cloud, energy-efficient and low-latency task offloading in edge computing, and CSI-based channel selection under partial observability for Wi-Fi data transmission. These diverse tasks highlight the versatility and robustness of the CORE framework in addressing key challenges in next-generation wireless network management and optimization.

A. Resource Allocation in ORAN-Cloud

In an ORAN-Cloud environment, a collection of servers \mathcal{M} deployed within the Centralized Unit (CU) manage various computational tasks, including Radio Resource Management (RRM), Control Plane Processing, Network Slicing,

and Machine Learning-based Inference. The CU supports diverse users such as User Equipment (UEs), Network Slices, Distributed Units (DUs), and External Network Services by dynamically allocating resources. When servers reach maximum capacity, incoming requests are temporarily queued, with adaptive load balancing to enhance efficiency.

Action Space: The discrete action space is denoted by \mathcal{A} , with cardinality $|\mathcal{A}| = 10$, involves selecting an appropriate server for each incoming task, $m \in \mathcal{M}$.

State Representation: The state space $\mathcal{S} \in \mathbb{R}^{3+4 \times |\mathcal{M}|}$ ($|\mathcal{M}| = 10$) encapsulates the following operational metrics:

- Demands of the incoming task (user request), including requirement of CPU (c_{req}) and RAM (r_{req}), as well as the estimated occupation time (t_{occ}).
- The CPU and RAM utilization rates on each server, represented as $U_{\text{cpu}} = \{u_{\text{cpu}}^m | m \in \mathcal{M}\}$ and $U_{\text{ram}} = \{u_{\text{ram}}^m | m \in \mathcal{M}\}$, which indicate the current resource load.
- The length of the pending queue in each server, represented as $L_{\text{queue}} = \{l_{\text{queue}}^m | m \in \mathcal{M}\}$, reflecting the count of pending tasks when CPU and RAM are used to handle other tasks.
- A queue penalty vector $P_{\text{queue}} = \{p_{\text{queue}}^m | m \in \mathcal{M}\}$ from each server. P_{queue} quantifies the delay-induced penalty associated with tasks, where $p_{\text{queue}}^m = \sum_i (c_{\text{req}}^i + r_{\text{req}}^i) \cdot t_{\text{occ}}^i$.

Reward Function: We seek to concurrently minimize power consumption and latency for users. The instantaneous power P_{power} is defined as in [26], while the delay penalty P_{latency} is computed as a normalized measure based on queuing penalties across all servers. For a set of M servers, we define:

$$r = -(w_1 \cdot P_{\text{power}} + w_2 \cdot P_{\text{latency}}) \quad (10)$$

$$= - \left(w_1 \cdot \sum_{m=1}^M (2u_{\text{cpu}}^m (u_{\text{cpu}}^m)^{1.4}) + w_2 \cdot \frac{p_{\text{queue}}^m}{\sum_{m \in \mathcal{M}} p_{\text{queue}}^m} \right). \quad (11)$$

Setup: The system begins with 1000 warm-up tasks, followed by 200 user requests. The reward function weights are set to $w_1 = 0.1$ and $w_2 = 0.2$, respectively.

B. Task Offloading in Edge Computing

Task offloading in edge computing delegates computational tasks from resource-constrained edge devices to more capable edge servers, thereby mitigating local power consumption while preserving acceptable processing latency. It is particularly crucial for managing image inference tasks on battery-powered edge devices, such as smartphones, where the computational demands of deep learning models can rapidly deplete limited energy resources. In our experiments, we explore task offloading for a variety of image-based inference tasks.

Action Space: The action space $\mathcal{A} = \{0, 1, 2, 3, 4\}$ includes five discrete options representing different offloading levels. Action $a = 0$ denotes full local execution on the client, while $a = 4$ corresponds to complete offloading to the server. Intermediate actions $a = 1, 2$, and 3 indicate offloading 25%, 50%, and 75% of the images, respectively.

State Representation: The state space $\mathcal{S} \in \mathbb{R}^{10}$ captures essential runtime information, including:

- A one-hot encoded vector indicating the current task type;
- Number of images in the current task;
- Average image size, represented as a 2D vector $[w, h]$;
- Remaining battery level of the client;
- GPU working frequency on the client device.

Reward Function: The delay T_{delay} is measured as the total processing time from the beginning to the end of a task. The remaining battery B_{remain} is calculated based on the input voltage and current over time. The reward r at each step is:

$$r = -(w_1 \cdot T_{\text{delay}} + w_2 \cdot (1 - B_{\text{remain}})). \quad (12)$$

Setup: The offloading task is built on the YOLOv11n series models [27]. We set $w_1 = 0.5$ and $w_2 = 1$. The client device is initialized with a random power level in the range [60,100]. Each task consists of several images, the number of which is sampled from the set $\{4, 8, 16, 24, 32\}$ with probabilities $\mathbf{p}_{\text{size}} = \{0.2, 0.2, 0.3, 0.2, 0.1\}$. The task type is randomly selected from five YOLOv11-based operations: detection, segmentation, classification, oriented bounding box (OBB) estimation, and pose estimation, based on the probability distribution $\mathbf{p}_{\text{type}} = \{0.25, 0.2, 0.2, 0.3, 0.05\}$. Each trajectory is terminated when the edge device has processed 200 tasks or can no longer operate due to battery depletion.

C. Channel Selection in Wi-Fi Communication

Adaptive channel selection is a widely adopted in Wi-Fi to enhance communication efficiency. Particularly, the transmitter dynamically selects a channel from a predefined candidates for packet transmission at a fixed rate. However, channel quality varies over time due to interference, fading, and mobility. To track these fluctuations, the receiver maintains a Channel State Information (CSI) table to log the most recent observations for each channel. The CSI is only updated when a channel is actively utilized.

Action Space: The action space consists of $n = 8$ discrete choices, $\mathcal{A} = \{1, 2, \dots, n\}$, each representing the selection of a specific wireless channel for data transmission.

State Representation: The state space, $\mathcal{S} \in \mathbb{R}^{53 \times |\mathcal{A}|}$, is defined as a 53-dimensional vector of CSI values corresponding to all channels. Since only the CSI of the currently used channel is updated, the agent hinges on historical CSI values for unselected channels, making the problem partially observable and temporally dependent.

Reward Function: At each step, the transmitter selects a new channel and starts sending packets at a fixed rate. The receiver collects incoming packets and tracks their sequence numbers. Once 100 packets (based on sequence numbers) have been received, the packet loss rate is calculated and used to define the reward:

$$r = -P_{\text{miss}}. \quad (13)$$

Setup: A total of eight channels are pre-defined, including five channels in the 5 GHz band (5.17 GHz, 5.20 GHz, 5.27 GHz, 5.32 GHz, and 5.72 GHz), and three in the 2.4 GHz

band (2.412 GHz, 2.442 GHz, and 2.472 GHz). Each trajectory consists of 200 steps.

VI. EVALUATION

This section describes the experiment setup, including real-world data collection, and presents experimental results to demonstrate the effectiveness of proposed CORE framework.

A. Experimental Setup

1) *Dataset Preparation:* We describe the process of collecting offline datasets for training across three use cases:

Resource Allocation: We implement the server resource allocation process in ORAN-Cloud using the Alibaba Cluster Trace v2018 dataset², an open-source collection of real cluster workloads. After that, we apply Greedy and Round-Robin policies to generate 1 million samples each. The Greedy policy selects the server with the fewest pending tasks, promoting better load balancing. For K-means, we set the cluster size to $k = 20,000$ with 1 expert sample per cluster.

Task Offloading: We employ both Greedy and Round-Robin policies to collect 50,000 samples each. The Greedy strategy makes decisions based on the client's remaining battery level to extend device longevity. Data collection takes approximately 52 hours for the Greedy and 46 hours for Round-Robin. For K-means, we set the cluster size to $k = 1,000$ and select 2 expert sample per cluster. The overall task offloading scenario between the edge client and server is illustrated in Fig. 3 (left).

Channel Selection: We collect 153,400 samples using a Round-Robin policy over 7 days of continuous transmission. For expert sample selection via K-means, we set the cluster size to $k = 2,000$, selecting one expert sample per cluster. The channel selection process for Wi-Fi signal transmission deployed on USRP is illustrated in Fig. 3 (right).



Fig. 3: Illustration of Task Offloading between edge client and server in an edge computing scenario (left) and Channel Selection for Wi-Fi signal transmission deployed on USRP (right).

2) *Algorithms Implementation:* For offline RL training, we focus mainly on CQL [28] and additional algorithms for comprehensive comparison, implemented from the offline Deep RL library D3RL³. These algorithms are chosen for their robust performance in offline settings with discrete action space. We also use two trajectory-based algorithms, CLUE [13] and OTR [29], as comparison baselines. The expert trajectories used in CLUE and OTR are selected based on the top higher trajectory returns. To ensure a fair comparison, we maintain the same size for expert samples.

²<https://github.com/alibaba/clusterdata>

³<https://github.com/takuseno/d3rlpy>

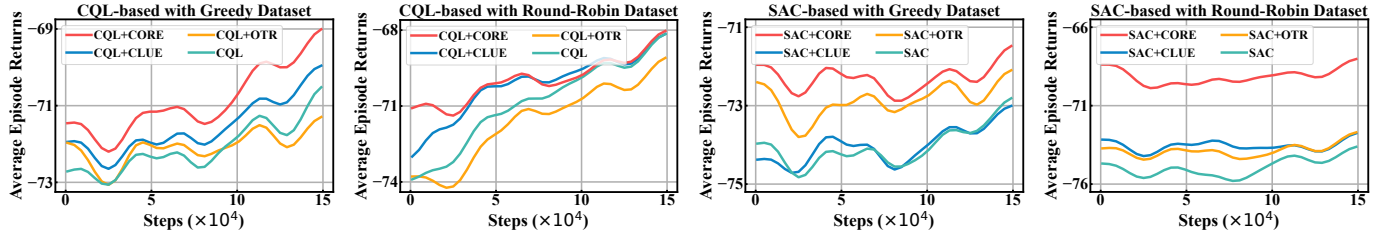


Fig. 4: Fine-tuning performances of CQL-based and SAC-based results on Greedy and Round-robin datasets in Resource Allocation.

3) *Enhanced CVAE*: The action embedding dimension is set to 8, corresponding to the discrete action space after embedding layer. The hidden dimension is configured to 128 for Resource Allocation and 64 for others. We set λ_{reg} to 40.0 to scale the regularization loss (Eq. 4) and λ_{neg} to 5.0 to scale the negative pair loss (Eq. 5). The m_e is specified by the margin parameter and is set to 0.3 (Eq. 5). We perform the training of the model over 20,000 iterations, with a batch size of 64. The learning rate (lr) is configured at 3e-4 with a weight decay of 0.0001 to regularize the weights during training.

4) *Offline Training*: We configure the offline training with following hyperparameters. The learning rate is 1e-4 with a batch size of 64. In CQL, the α is 1.0. The discount factor γ is 0.9 for task offloading and 0.8 for others. The Adam optimizer employs a weight decay of 5e-5. The neural network comprises a two-layer encoder with hidden dimensions of 64, incorporating batch normalization and a dropout rate of 0.2. The Q-function adopts a quantile regression approach with 100 quantiles. Training is performed using five distinct random seeds, with five trials per seed, resulting in 25 trials. The reported results are averaged across all trials to ensure robustness and reliability.

B. Results on Resource Allocation

We evaluate CORE for resource allocation in ORAN-Cloud. For the offline training phase, we undertake a substantial 5e5 steps to comprehensively train the models. Subsequently, the models are fine-tuned for an additional 150,000 steps in the online system to further optimize their performance.

1) *Comparison with Baselines*: Fig. 4 compares the performance of CORE against baselines during online fine-tuning. The configuration with $k = 20,000$ clusters and a τ value of 0.3 achieves the highest returns. Across all results, CORE consistently outperforms the baselines with the highest average returns. In contrast to trajectory-level approaches like CLUE and OTR, CORE leverages a state-based expert selection mechanism, allowing for more granular and context-aware identification of valuable samples in the dataset.

Additionally, Fig. 5 presents an analysis of the resultant reward distribution, emphasizing the effect of applying different values of τ (See Eq. 9) on the distribution of rewards after integration. When $\tau = 0.0$, the distribution peaks around -0.8 and exhibits a relatively high probability density in this region. As τ increases to 0.3, the peak of the distribution shifts slightly to the right, around -0.7. The distribution shifts observed with different τ values confirm that scaling the compensation reward effectively adjusts the reward distribution.

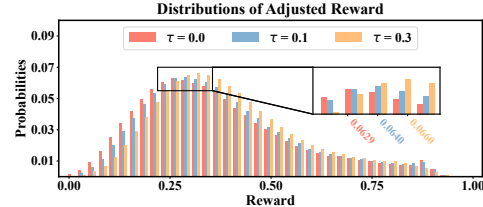


Fig. 5: Distributions in adjusted reward distributions for different τ scales in the Greedy dataset ($k = 20,000$). Notes: $\tau = 0.0$ represents using the original rewards in dataset.

TABLE I: Average step rewards comparison of CQL with CORE across different K-means cluster sizes (k) and τ parameters in Greedy and Round-Robin datasets after offline training phase.

	τ	Greedy	Round-Robin
CQL+CORE ($k = 2,500$)	0.1	-0.356 ± 0.0276	-0.3595 ± 0.0274
	0.3	-0.3538 ± 0.0259	-0.3533 ± 0.0266
CQL+CORE ($k = 5,000$)	0.1	-0.3555 ± 0.027	-0.3565 ± 0.0276
	0.3	-0.3537 ± 0.0287	-0.3499 ± 0.0281
CQL+CORE ($k = 10,000$)	0.1	-0.355 ± 0.0274	-0.3542 ± 0.0263
	0.3	-0.3537 ± 0.0258	-0.3492 ± 0.0285
CQL+CORE ($k = 20,000$)	0.1	-0.3551 ± 0.0272	-0.3556 ± 0.0283
	0.3	-0.3537 ± 0.0263	-0.3474 ± 0.0277

2) *Parameters Optimization*: Tab. I provides a detailed comparison of performance improvements after offline training with additional clustering. The results are shown for different scaling factors τ under both Greedy and Round-Robin datasets. Significantly, with an increasing number of clusters, the integration of CORE consistently improves average step rewards. The most significant gains are observed with $\tau = 0.3$, at the largest cluster size of 20,000. This highlights the optimal hyperparameter settings for CORE, demonstrating that a higher cluster size and a τ value of 0.3 yield the best performance across both algorithms and datasets. These findings emphasize the importance of selecting appropriate hyperparameters to enhance learning efficiency. Such improvements suggest that CORE can effectively leverage clustering to optimize performance, providing a promised framework for real-world network tasks.

3) *Adaptability of CORE*: Tab. II compares offline RL algorithms w/o CORE with parameters $k = 20,000$ and $\tau = 0.3$ in Greedy and Round-Robin datasets. CORE consistently improves the performance of DDQN [30], BCQ [31], and SAC [32] in both datasets. Remarkably, the performance gains are statistically significant in most cases as indicated by p -values. These results validate the effectiveness and generality of CORE in enhancing offline RL.

TABLE II: Performance comparison of offline RL algorithms. \uparrow indicates improvement over the base method. Reported p -values are calculated using the independent t-test.

		DDQN	BCQ	SAC
Dataset	Greedy	-0.3574	-0.3583	-0.3602
	Greedy+CORE	-0.3556\uparrow	-0.3543	-0.3523\uparrow
	p -value	5.96e-3	5.94e-2	2.07e-5
	Round-Robin	-0.3544	-0.3634	-0.362
	Round-Robin+CORE	-0.3424\uparrow	-0.3531\uparrow	-0.3348\uparrow
	p -value	2.32e-12	6.01e-9	1.12e-39

4) *Ablation for CVAE model:* The ablation study results ($k = 20,000, \tau = 0.3$) elucidate the significant impact of regularization and contrastive components on the performance of our enhanced CVAE. As shown in Fig. 6, the complete model that incorporates the regularization loss \mathcal{L}_{reg} and the contrastive loss \mathcal{L}_{contra} consistently outperforms variants that lack either of them. This is indicated by marked improvements in average rewards. Statistical significance further validates the importance of these loss components. Additionally, the CVAE training behavior illustrates that incorporating the negative pair loss \mathcal{L}_{neg} leads to a rapid reduction, thereby indicating its contribution to the model’s faster and more accurate convergence than only involving regularization loss \mathcal{R}_{reg} .

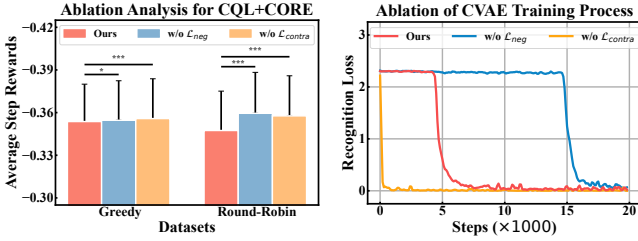


Fig. 6: Ablation study on the CQL+CORE’s performance across Greedy and Round-Robin datasets (left), along with CVAE training convergence (right) on Round-Robin dataset. Significance is noted (* p -value < 0.05 , *** p -value < 0.001).

Beyond numerical performance, we further investigate how CORE affects system-level behavior under different training datasets and workload conditions. Fig. 7 (left) shows that different training datasets lead to distinct latency and energy patterns with the increase of user numbers, which highlights how dataset choice influences system behavior. Fig. 7 (right) shows that the CORE consistently improves performance compared to the underlying baseline behaviors. The observed reward gap indicates that CORE effectively learns better policies regardless of the data source, demonstrating its robustness and adaptability across workload levels.

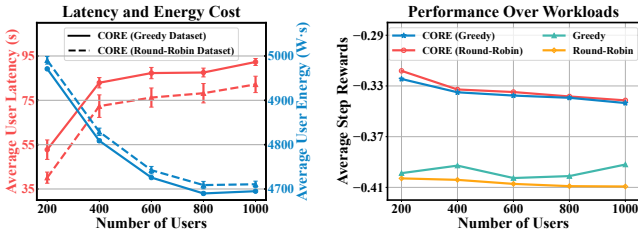


Fig. 7: Different datasets lead to varying latency and energy profiles (left). The CORE algorithm consistently improves performance over baseline behaviors (right).

C. Results on Task Offloading

We evaluate CORE in a practical image task offloading, as illustrated in Fig. 3 (left). We perform a total of $2e4$ training steps given the limited dataset size of $5e4$ samples. This dataset is significantly smaller than typical offline datasets.

1) *Comparison with Baselines:* Tab III presents the average trajectory returns of various methods trained on Greedy and Round-Robin datasets. From Tab III, CORE consistently outperforms all baselines across both datasets, achieving the highest average returns with the lowest variance. This indicates the effectiveness and stability of our method under different data generation strategies for task offloading. In addition, our results on the Round-Robin dataset are generally better than those on the Greedy dataset across all methods. This is likely because Round-Robin generates more uniformly distributed actions and experiences, which offers a better initial coverage for offline learning. It is worth noting that both CLUE and OTR hinge on identifying expert trajectories, which limits their performance when expert demonstrations are sparse or absent. In contrast, CORE is more robust and better suited to limited datasets via leveraging state-based advantage estimation. Such results support is consistent with our claim that CORE offers a more scalable and data-efficient solution.

TABLE III: Average trajectory returns comparison among baselines in Greedy and Round-Robin datasets.

	Greedy	Round-Robin
CQL	-187.8068 ± 1.3229	-127.2304 ± 1.9439
CQL+OTR	-192.0710 ± 2.6662	-128.0848 ± 2.4420
CQL+CLUE	-215.0105 ± 18.3347	-129.3592 ± 3.1457
CQL+CORE	-181.9689 ± 1.0237	-125.1219 ± 1.6114

2) *Performance under Shifted Workload Distributions:* To evaluate the generalization ability of CORE and baselines beyond the training data distribution, we examine their performance under three OOD task workloads characterized by distinct image size sampling probabilities. Specifically, we define the sampling probabilities as follows: $p_{size} = \{0.3, 0.3, 0.2, 0.1, 0.1\}$ (expected size: 12.4) for the *light workload*; $p_{size} = \{0.15, 0.3, 0.15, 0.3, 0.1\}$ (expected size: 15.8) for the *moderate workload*; $p_{size} = \{0.2, 0.1, 0.2, 0.1, 0.4\}$ (expected size: 20.0) for the *heavy workload*. These distributions deviate significantly from the one used during offline dataset collection, thereby introducing substantial shifts in workload characteristics. As shown in Fig. 8 (next page), CORE consistently surpasses all baselines across these unseen workload settings with the highest average returns in all three cases. This result highlights CORE’s robustness and its ability to generalize effectively to dynamic and heterogeneous task distributions in real-world task offloading in edge computing.

D. Results on Channel Selection

We deploy CORE for channel selection in Wi-Fi transmission on USRP as shown in Fig. 3 (right). The receiver decodes the signal in real time. The signal quality is monitored via the MAC frame logs, time-domain signals, and the constellation diagram. We perform a total of $5e4$ offline training steps given the dataset size of 153,400.

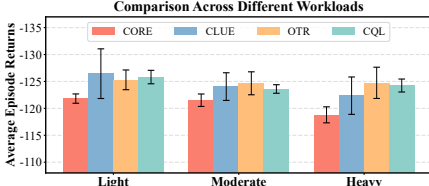


Fig. 8: Performance comparison under three unseen task distributions in Task Offloading.

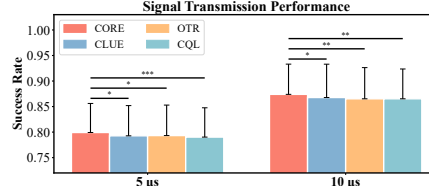


Fig. 9: Signal Transmission Evaluation. Significance is noted (* p -value < 0.05, ** p -value < 0.01, *** p -value < 0.001).

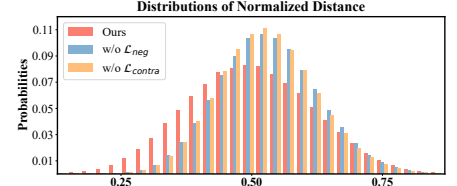


Fig. 10: Illustration of normalized distance distributions: ours (CORE), without the negative loss, and without the contrastive loss.

1) *Comparison with Baselines*: We use the packet success rate as the evaluation metric, which is measured based on real-time packet reception. We calculate the p-values using an independent two-sample t-test based on results collected over 5,000 environment steps within 5 random seeds. As shown in Fig. 9, CORE consistently achieves significantly higher packet success rates than the baseline methods across different transmission intervals, (5 μ s and 10 μ s). Under a 5 μ s packet transmission interval, CORE achieves a success rate of 0.7992, dramatically outperforming CLUE (p -value = 0.0099), OTR (p -value = 0.0235), and CQL (p -value = 0.0004). The improvements remain obvious under the 10 μ s interval, compared to CLUE (p -value = 0.0291), OTR (p -value = 0.0012), and CQL (p -value = 0.0012). These results validate the effectiveness of CORE in enhancing robustness and reliability in practical signal transmission.

2) *Ablation Study on Distance Distribution in CVAE’s Latent Space*: To explore the effectiveness of compensable reward mechanism, we analyze the latent distance distributions. Fig. 10 visualizes the normalized distances between expert and non-expert samples in the latent space under three variants: ours, the model without the negative loss (w/o neg, the same CVAE design as CLUE), and the model without the contrastive loss (w/o contra, standard CVAE). We observe that our method yields a noticeably broader distance distribution compared to the ablated baselines. In contrast, both ablated versions tend to collapse the distance range, leading to a less informative signal for reward compensation. The broader distribution implies that our model provides a more fine-grained and expressive measurement of behavioral discrepancy, which enhances the resolution of the compensable reward. This finding demonstrates that a better-separated latent representation achieves more useful internal feedback, facilitating robust learning from suboptimal and limited offline data.

VII. RELATED WORKS

In offline RL, there is a growing interest in using expert samples for sparse-reward or reward-free data [33], [34]. Offline Imitation Learning (IL) methods, such as Behavior Cloning (BC) [35] and offline Inverse Reinforcement Learning (IRL) [36], learn from expert and suboptimal offline data. BC maps states to actions based on expert samples, treating policy learning as a supervised learning problem [37]. Methods like Generative Adversarial Imitation Learning (GAIL) have shown success but face challenges with sample efficiency and optimization [38]. Recent advancements, such as OTR [29]

and Primal Wasserstein Imitation Learning (PWIL) [39], aim to align the distance between expert and agent state-action distributions. Innovative methods like CLUE bind expert data embeddings to learn calibrated task-oriented behaviors [13], enhancing policy learning from static datasets and reducing the need for extensive online interactions. However, these advancements heavily rely on the availability and quality of expert data, which is often laborious and costly to obtain in real-world applications.

The application of offline RL in real world has attracted increasing attention. For example, CQL has been adopted for computation offloading in augmented reality (AR) environments [8], while other algorithms have also been explored for wireless radio resource management (RRM) [2]. A notable system-level effort is OpenRAN Gym⁴, an AI/ML platform for intelligent ORAN, which incorporates a full offline RL pipeline [40] and supports model deployment for online fine-tuning [41]. However, most of them stop at directly applying existing algorithms to domain-specific tasks, without delving into how to better align offline RL methods with the unique features and constraints of real-world applications. Furthermore, few follow-up works have extended or systematically built upon these pipelines [42], [43], revealing a critical gap in the development of generalizable and deployable offline RL solutions, particularly within the wireless network domain.

VIII. CONCLUSIONS

In this paper, we propose CORE, a novel offline RL framework that enhances policy learning by enlarging reward discrepancies within compensable rewards. CORE identifies and distinguishes expert from non-expert behaviors to broaden reward distribution. To this end, CORE enables effective learning guidance, especially given imperfect offline datasets. We validated CORE extensively in three representative wireless network use cases using data collected from real world. Our experimental results indicate that CORE consistently outperforms baseline methods, indicating its robustness in diverse wireless network tasks. CORE not only yields strong overall performance, but also remains effective in data-scarce scenarios. For example, in the task offloading with merely 50,000 samples, CORE achieves substantial improvements over all baselines. These findings highlight CORE’s practicality in real-world scenarios with limited expert data, rendering it a generalizable and scalable solution for wireless network management and optimization.

⁴<https://openrangenlgym.com/>

REFERENCES

[1] D. C. Nguyen, P. Cheng, M. Ding, D. Lopez-Perez, P. N. Pathirana, J. Li, A. Seneviratne, Y. Li, and H. V. Poor, "Enabling ai in future wireless networks: A data life cycle perspective," *IEEE Communications Surveys and Tutorials*, vol. 23, no. 1, pp. 553–595, 2021.

[2] K. Yang, C. Shi, C. Shen, J. Yang, S.-p. Yeh, and J. J. Sydir, "Offline reinforcement learning for wireless network optimization with mixture datasets," *IEEE Transactions on Wireless Communications*, 2024.

[3] L. Bonati, M. Polese, S. D’Oro, S. Basagni, and T. Melodia, "OpenRAN Gym: An Open Toolbox for Data Collection and Experimentation with AI in O-RAN," in *Proc. of IEEE WCNC Workshop on Open RAN Architecture for 5G Evolution and 6G*, Austin, TX, USA, April 2022.

[4] J. Tan, R. Khalili, H. Karl, and A. Hecker, "Multi-agent distributed reinforcement learning for making decentralized offloading decisions," in *IEEE INFOCOM 2022 - IEEE Conference on Computer Communications*, 2022, pp. 2098–2107.

[5] N. Yang, S. Chen, H. Zhang, and R. Berry, "Beyond the edge: An advanced exploration of reinforcement learning for mobile edge computing, its applications, and future research trajectories," *IEEE Communications Surveys and Tutorials*, vol. 27, no. 1, pp. 546–594, 2025.

[6] K. Yang, C. Shi, C. Shen, J. Yang, S.-P. Yeh, and J. J. Sydir, "Offline reinforcement learning for wireless network optimization with mixture datasets," *IEEE Transactions on Wireless Communications*, vol. 23, no. 10, pp. 12 703–12 716, 2024.

[7] R. Figueiredo Prudencio, M. R. O. A. Maximo, and E. L. Colombini, "A survey on offline reinforcement learning: Taxonomy, review, and open problems," *IEEE Transactions on Neural Networks and Learning Systems*, vol. 35, no. 8, pp. 10 237–10 257, 2024.

[8] S. Zhao, W. Jing, F. R. Yu, X. Wen, and Z. Lu, "Mobility-aware computation offloading for ai tasks over terahertz wireless networks: An offline reinforcement learning approach," *IEEE Transactions on Vehicular Technology*, 2024.

[9] S. Levine, A. Kumar, G. Tucker, and J. Fu, "Offline reinforcement learning: Tutorial, review, and perspectives on open problems," *arXiv preprint arXiv:2005.01643*, 2020.

[10] D. Qiao and Y.-X. Wang, "Offline reinforcement learning with differential privacy," in *Proceedings of the 37th International Conference on Neural Information Processing Systems*, ser. NIPS ’23. Red Hook, NY, USA: Curran Associates Inc., 2023.

[11] K. Hippalgaonkar, Q. Li, X. Wang, J. W. Fisher III, J. Kirkpatrick, and T. Buonassisi, "Knowledge-integrated machine learning for materials: lessons from gameplaying and robotics," *Nature Reviews Materials*, vol. 8, no. 4, pp. 241–260, 2023.

[12] K. Yan, A. Schwing, and Y.-X. Wang, "A simple solution for offline imitation from observations and examples with possibly incomplete trajectories," *Advances in Neural Information Processing Systems*, vol. 36, 2024.

[13] J. Liu, L. Zu, L. He, and D. Wang, "Clue: Calibrated latent guidance for offline reinforcement learning," in *Conference on Robot Learning*. PMLR, 2023, pp. 906–927.

[14] C. Jin, A. Krishnamurthy, M. Simchowitz, and T. Yu, "Reward-free exploration for reinforcement learning," in *International Conference on Machine Learning*. PMLR, 2020, pp. 4870–4879.

[15] R. F. Prudencio, M. R. Maximo, and E. L. Colombini, "A survey on offline reinforcement learning: Taxonomy, review, and open problems," *IEEE Transactions on Neural Networks and Learning Systems*, 2023.

[16] K. Sohn, H. Lee, and X. Yan, "Learning structured output representation using deep conditional generative models," *Advances in neural information processing systems*, vol. 28, 2015.

[17] Y. Wang, C. Yang, Y. Wen, Y. Liu, and Y. Qiao, "Critic-guided decision transformer for offline reinforcement learning," in *Proceedings of the AAAI Conference on Artificial Intelligence*, vol. 38, no. 14, 2024, pp. 15 706–15 714.

[18] A. Rajeswaran, V. Kumar, A. Gupta, G. Vezzani, J. Schulman, E. Todorov, and S. Levine, "Learning complex dexterous manipulation with deep reinforcement learning and demonstrations," 2018.

[19] E. Todorov, T. Erez, and Y. Tassa, "Mujoco: A physics engine for model-based control," in *2012 IEEE/RSJ International Conference on Intelligent Robots and Systems*. IEEE, 2012, pp. 5026–5033.

[20] J. Fu, A. Kumar, O. Nachum, G. Tucker, and S. Levine, "D4rl: Datasets for deep data-driven reinforcement learning," 2020.

[21] J. Schulman, F. Wolski, P. Dhariwal, A. Radford, and O. Klimov, "Proximal policy optimization algorithms," *arXiv preprint arXiv:1707.06347*, 2017.

[22] V. Balazadeh, K. Chidambaram, V. Nguyen, R. G. Krishnan, and V. Syrgkanis, "Sequential decision making with expert demonstrations under unobserved heterogeneity," *Advances in Neural Information Processing Systems*, vol. 37, pp. 65 476–65 498, 2024.

[23] Z. Zheng, J. Oh, M. Hessel, Z. Xu, M. Kroiss, H. Van Hasselt, D. Silver, and S. Singh, "What can learned intrinsic rewards capture?" in *International Conference on Machine Learning*. PMLR, 2020, pp. 11 436–11 446.

[24] R. Dadashi, L. Hussenot, M. Geist, and O. Pietquin, "Primal wasserstein imitation learning," 2021. [Online]. Available: <https://arxiv.org/abs/2006.04678>

[25] S. Fujimoto, H. Hoof, and D. Meger, "Addressing function approximation error in actor-critic methods," in *International conference on machine learning*. PMLR, 2018, pp. 1587–1596.

[26] N. Liu, Z. Li, J. Xu, Z. Xu, S. Lin, Q. Qiu, J. Tang, and Y. Wang, "A hierarchical framework of cloud resource allocation and power management using deep reinforcement learning," in *2017 IEEE 37th international conference on distributed computing systems (ICDCS)*. IEEE, 2017, pp. 372–382.

[27] R. Khanam and M. Hussain, "Yolov11: An overview of the key architectural enhancements," 2024.

[28] A. Kumar, A. Zhou, G. Tucker, and S. Levine, "Conservative q-learning for offline reinforcement learning," *Advances in Neural Information Processing Systems*, vol. 33, pp. 1179–1191, 2020.

[29] Y. Luo, Z. Jiang, S. Cohen, E. Grefenstette, and M. P. Deisenroth, "Optimal transport for offline imitation learning," 2023. [Online]. Available: <https://arxiv.org/abs/2303.13971>

[30] H. Van Hasselt, A. Guez, and D. Silver, "Deep reinforcement learning with double q-learning," in *Proceedings of the AAAI conference on artificial intelligence*, vol. 30, no. 1, 2016.

[31] S. Fujimoto, D. Meger, and D. Precup, "Off-policy deep reinforcement learning without exploration," in *International conference on machine learning*. PMLR, 2019, pp. 2052–2062.

[32] T. Haarnoja, A. Zhou, K. Hartikainen, G. Tucker, S. Ha, J. Tan, V. Kumar, H. Zhu, A. Gupta, P. Abbeel, et al., "Soft actor-critic algorithms and applications," *arXiv preprint arXiv:1812.05905*, 2019.

[33] A. Block, A. Jadbabaie, D. Pfrommer, M. Simchowitz, and R. Tedrake, "Provable guarantees for generative behavior cloning: Bridging low-level stability and high-level behavior," *Advances in Neural Information Processing Systems*, vol. 36, pp. 48 534–48 547, 2023.

[34] Q. Li, J. Zhang, D. Ghosh, A. Zhang, and S. Levine, "Accelerating exploration with unlabeled prior data," *Advances in Neural Information Processing Systems*, vol. 36, 2024.

[35] D. J. Foster, A. Block, and D. Misra, "Is behavior cloning all you need? understanding horizon in imitation learning," *arXiv preprint arXiv:2407.15007*, 2024.

[36] S. Zeng, C. Li, A. Garcia, and M. Hong, "When demonstrations meet generative world models: A maximum likelihood framework for offline inverse reinforcement learning," *Advances in Neural Information Processing Systems*, vol. 36, pp. 65 531–65 565, 2023.

[37] L. Ke, J. Wang, T. Bhattacharjee, B. Boots, and S. Srinivasa, "Grasping with chopsticks: Combating covariate shift in model-free imitation learning for fine manipulation," in *2021 IEEE International Conference on Robotics and Automation (ICRA)*. IEEE, 2021, pp. 6185–6191.

[38] J. Ho and S. Ermon, "Generative adversarial imitation learning," *Advances in neural information processing systems*, vol. 29, 2016.

[39] R. Dadashi, L. Hussenot, M. Geist, and O. Pietquin, "Primal wasserstein imitation learning," *arXiv preprint arXiv:2006.04678*, 2020.

[40] L. Bonati, M. Polese, S. D’Oro, S. Basagni, and T. Melodia, "Openran gym: Ai/ml development, data collection, and testing for o-ran on pawr platforms," *Computer Networks*, vol. 220, p. 109502, 2023.

[41] L. Bonati, M. Polese, S. D’Oro, S. Basagni, and T. Melodia, "Intelligent closed-loop ran control with xapps in openran gym," in *27th European Wireless Conference*. VDE, 2022, pp. 1–6.

[42] C. Fiandrino, L. Bonati, S. D’Oro, M. Polese, T. Melodia, and J. Widmer, "Explora: Ai/ml explainability for the open ran," *Proceedings of the ACM on Networking*, vol. 1, no. CoNEXT3, pp. 1–26, 2023.

[43] P. Li, J. Thomas, X. Wang, A. Khalil, A. Ahmad, R. Inacio, S. Kapoor, A. Parekh, A. Doufexi, A. Shojaeifard, et al., "Rlops: Development life-cycle of reinforcement learning aided open ran," *IEEE Access*, vol. 10, pp. 113 808–113 826, 2022.